Elsevier required licence: ©2023. This manuscript version is made available under the CCBY-NC-ND 4.0 license http://creativecommons.org/licenses/by-nc-nd/4.0/ The definitive publisher version is available online at https://doi.org/10.1016/j.jallcom.2023.170983

Bandgap narrowing and hole self-trapping reduction in Ga_2O_3 by Bi_2O_3 alloying

Fatima Matar[a], Ying-Li Shi[b,c], Francis Chi-Chung Ling[b], Amar Salih[a], Curtis P. Irvine[a], Sujeewa De Silva[a], Matthew R. Phillips[a], and Cuong Ton-That[a,*]

[a] *School of Mathematical and Physical Sciences, University of Technology Sydney, Ultimo, New South Wales 2007, Australia*

[b] *Department of Physics, The University of Hong Kong, Pokfulam, Hong Kong 999077, PR China*

[c] *Department of Electrical and Electronics Engineering, Xi'an Jiaotong-Liverpool University, Suzhou 215000, PR China*

* Corresponding author: cuong.ton-that@uts.edu.au

Abstract

Ga_2O_3 is an emerging material with attractive electrical properties for improving the performance of high-voltage power electronics, and it is widely accepted that engineering its band edge energies will expand its applications, especially for bipolar devices. In this work, monoclinic phase $(Bi_xGa_{1-x})_2O_3$ ternary alloys are fabricated on *c*-plane sapphire via magnetron co-sputtering of Ga_2O_3 and Bi_2O_3. The bandgap of Ga_2O_3 is found to decrease from 4.97 to 4.78 eV by alloying with a Bi x-fraction of 0.04, consistent with the theoretical prediction that alloying with Bi_2O_3 causes the up-shift of the valence band. Concurrent temperature-resolved cathodoluminescence (CL) measurements of the Ga_2O_3 and $(Bi_{0.04}Ga_{0.96})_2O_3$ are employed to investigate their intrinsic UV luminescence and defect-related visible bands with increasing temperature from 80 K. The CL results reveal a more rapid thermal quenching of the self-trapped hole emission with an activation energy of only 32 meV, suggesting that alloying with Bi_2O_3 lowers the self-trapping energy for holes. Temperature-dependent electrical measurements reveal the conductivity of the $(Bi_{0.04}Ga_{0.96})_2O_3$ film is one order of magnitude lower than that of the undoped Ga_2O_3 counterpart; however, both possess an electrical activation energy of ~ 26 meV, likely associated with an impurity-related shallow donor. While the low electrical conductivity of $(Bi_{0.04}Ga_{0.96})_2O_3$ can be attributed to the compensation of shallow donors

by acceptors activated by the Bi_2O_3-induced upward shift of the valence band edge. The frequency-dependent conduction and ionic polarization mechanisms up to 10^7 Hz are found to be identical for Ga_2O_3 and $(Bi_{0.04}Ga_{0.96})_2O_3$, indicating that the conduction in this ternary alloy does not involve the activation of Bi acceptors.

Keywords: gallium oxide; bismuth; alloying; self-trapped holes; electrical conductivity

1. Introduction

Ga_2O_3 is a promising material for high-power electronic devices because it possesses an estimated breakdown field of 8 MV/cm, substantially greater than the semiconductors currently used in the high-power electric device industry, namely SiC (2.5 MV/cm) and Si (0.3 MV/cm) [1]. Additionally, it is expected that the ultra-wide bandgap and high thermal stability of Ga_2O_3 will facilitate the fabrication of a wide range of transparent electronic components and electroluminescent devices as well as gas sensors, all capable of operating at elevated temperatures. Development of Ga_2O_3-based electronics, particularly for bipolar devices, requires both n-type and p-type doped Ga_2O_3. Monoclinic phase β-Ga_2O_3 is an n-type semiconductor due to the presence of (i) native oxygen vacancy (V_O) donors and (ii) donor impurities such as Si and H inadvertently incorporated during growth [2-4]. While precisely controlled n-type conductivity in β-Ga_2O_3 is achieved by substitutional cation doping with Si, Ge or Sn that acts as a shallow donor [5, 6]. Conversely, achieving p-type conductivity in Ga_2O_3 remains challenging due to the difficulty in finding suitable shallow acceptors, compensation of acceptors by native defects, the large effective mass of holes, and especially its low-lying valence band (VB) maximum [7]. One way to overcome this impediment is through bandgap engineering. Alloying is frequently used for bandgap engineering and tailoring the physical and electronic structure to suit particular applications. Introducing Al_2O_3 or In_2O_3 into Ga_2O_3 thin films in pulsed laser deposition (PLD) has been successfully employed to alter the bandgap, allowing the fabrication

of Ga_2O_3 alloys with a wide range of bandgap from 3.6 to 6.8 eV [8-10]. Another promising approach is sputter deposition of Ga_2O_3 thin films in NH_3 atmosphere to produce gallium oxynitride (GaON) with a reduced bandgap down to about 2.1 eV [11]. However, a broad range of β-phase Ga_2O_3 alloys is difficult to obtain due to the high anisotropy of the monoclinic structure and the lattice mismatch with sapphire substrates causing phase separation and an amorphous structure even with a small alloy concentration [12, 13]. A recent computational study based on density functional theory (DFT) calculations proposes that the introduction of Bi in the form of $(Bi_xGa_{1-x})_2O_3$ alloy would raise the VB edge energy without introducing significant structural distortions [14]. This intermediate VB, composed of Bi 6s and O 2p orbitals, could potentially reduce the binding energy of acceptor dopants, allowing the realization of stable p-type doping of β-Ga_2O_3. However, experimental research on $(Bi_xGa_{1-x})_2O_3$ alloys is still in its infancy. In this work, monoclinic phase $(Bi_{0.04}Ga_{0.96})_2O_3$ thin films are successfully grown via radio frequency (RF) magnetron co-sputtering and post-growth annealing. This paper presents the results of detailed investigations into β-$(Bi_{0.04}Ga_{0.96})_2O_3$ using microstructural, optical and electrical analyses. The results show that Bi_2O_3 alloying is a viable approach to tailor the electronic band structure and to reduce the energetics of hole self-trapping in Ga_2O_3.

2. Experimental details

$(Bi_xGa_{1-x})_2O_3$ alloy and Ga_2O_3 films of 300 nm thickness were fabricated on the *c*-plane sapphire substrate by radio frequency (RF) magnetron sputtering of Ga_2O_3 and Bi_2O_3 ceramic targets (both with 99.99% purity) in an Ar/O_2 80/20 gas mixture, and then annealed at 800°C in Ar gas for 1 hour. Before deposition, the substrate was cleaned in acetone, isopropanol, and deionized water in an ultrasonic bath for 10 minutes for each step, followed by blow-drying with N_2 gas. The substrate was rotated at 10 rpm during deposition. The deposition chamber had a base pressure of 2×10^{-5} Torr and the working pressure during deposition was 2.9×10^{-3} Torr. Constant RF powers of 100 W and 10 W

were applied to the Ga_2O_3 and Bi_2O_3 targets, respectively. Investigations of the film morphology and elemental composition were carried out using Atomic Force Microscopy (AFM) with a Park XE7 instrument and Energy Dispersive X-ray (EDX) spectroscopy using a Bruker Quantax 400 system, respectively. X-ray diffraction (XRD) was performed on a Bruker D8 Discovery diffractometer using Cu Kα radiation. The optical properties of the films were characterized using an Agilent Cary 7000 UV-Vis spectrophotometer. Temperature-dependent CL spectroscopy was performed using FEI Quanta SEM equipped with a QE65000 spectrometer and a liquid N_2 temperature-controlled cryostat stage. All CL spectra were corrected for the total system response. For electrical and dielectric measurements, the oxide films were deposited on the erbium-doped zinc oxide (ErZO) film and a vertical device structure of Al/Ga_2O_3/ErZO/sapphire substrate was employed as described in our previous work [15]. The Al top electrodes (lateral dimensions of 1 mm × 1 mm and thickness of 120 nm) were deposited through a shallow mask. Temperature-dependent direct current (DC) conductivity measurements were conducted using Keithley 2601B, while the alternating current (AC) and dielectric properties were analyzed in the frequency range of 20 Hz to 10 MHz using a Keysight E4990A impedance analyzer.

3. Results and Discussion

3.1 Structural properties of $(Bi_{0.04}Ga_{0.96})_2O_3$ films

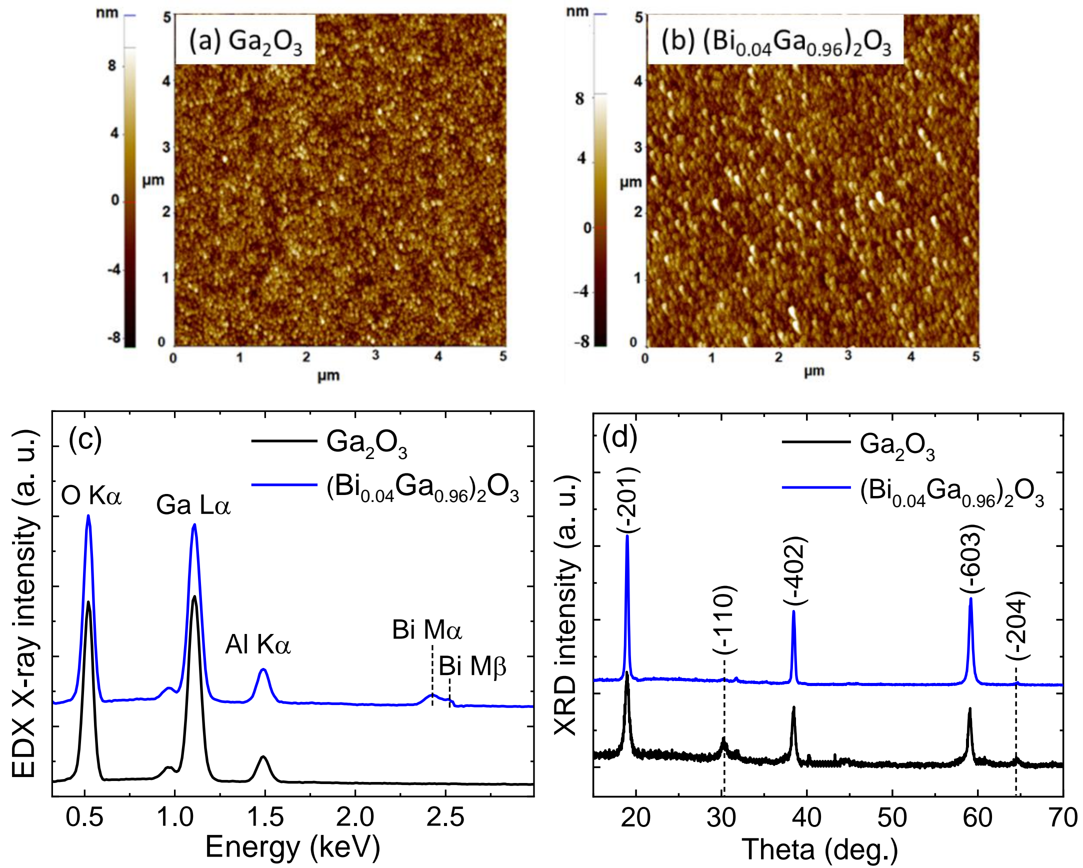

Figure 1. AFM images of (a) Ga_2O_3 and (b) $(Bi_{0.04}Ga_{0.96})_2O_3$ films, with a RMS roughness of 2.3 ± 0.3 nm and 2.6 ± 0.5 nm for Ga_2O_3 and $(Bi_{0.04}Ga_{0.96})_2O_3$ films, respectively. (c) EDX spectra of the films showing the additional Bi Mα an Mβ peaks in the doped film. (d) XRD patterns of the Ga_2O_3 and $(Bi_{0.04}Ga_{0.96})_2O_3$ films showing the $(\bar{2}01)$ surface orientation with all the peaks indexed to the monoclinic phase.

Figure 1(a, b) depicts the AFM images of the Ga_2O_3 and $(Bi_{0.04}Ga_{0.96})_2O_3$ films, both exhibit fine nanocrystalline structures with grain sizes of tens of nm. The root mean square (RMS) roughness, measured over a surface area of 5×5 μm^2, is 2.3 nm and 2.6 nm for the Ga_2O_3 to $(Bi_xGa_{1-x})_2O_3$ films, respectively. Figure 1(c) represents the EDX spectra acquired with a beam energy of 5 kV, which display characteristic Ga and O X-ray peaks in the undoped samples corresponding to Ga_2O_3 in

addition to the Bi peak identified in the alloy film. The presence of an Al peak arises from the sapphire substrate. Two Bi Mα and Mβ X-ray peaks are clearly visible in the alloy spectrum. EDX analysis using Aztec software (Oxford Instruments) yields a Bi x-fraction of 0.040 ± 0.006 in $(Bi_xGa_{1-x})_2O_3$. The XRD patterns of the films, presented in Figure 1(d), show characteristics of high-quality monoclinic structure. Three dominant sharp peaks at 19.0, 38.5 and 59.2° can be indexed to $(\bar{2}01)$, $(\bar{4}02)$ and $(\bar{6}03)$ planes of β-Ga_2O_3, which is previously attributed to the similarity in the oxygen arrangements of the monoclinic $(\bar{2}01)$ plane and the c-sapphire surface [16]. The similarity of the two XRD patterns and the absence of peaks associated with other Ga_2O_3 polymorphs indicate that the monoclinic phase structure is preserved in the alloy film. The Ga_2O_3 film also shows weak diffraction peaks belonging to $(\bar{1}10)$ and $(\bar{2}04)$ planes, while the XRD pattern of the $(Bi_{0.04}Ga_{0.96})_2O_3$ consists of only peaks belonging to the $(\bar{2}01)$ plane family. The predominant growth of the $(Bi_{0.04}Ga_{0.96})_2O_3$ film along the [201] direction suggests the alloy film becomes more commensurate with the substrate lattice. No characteristic diffraction peaks related to Bi or BiO_x are identifiable in XRD, which suggests that Bi atoms are well incorporated into the monoclinic crystal structure of the film. Using the full width at half maximum (FWHM) of the $(\bar{2}01)$ diffraction peak and the Scherrer equation, the average crystallite size is calculated to be 14 and 25 nm for the Ga_2O_3 and $(Bi_{0.04}Ga_{0.96})_2O_3$ films, respectively. This result is in accordance with the observation of grain size enlargement due to the Bi_2O_3 alloying shown in Figure 1(a, b).

3.2 Influence of Bi_2O_3 alloying on the bandgap and self-trapped holes

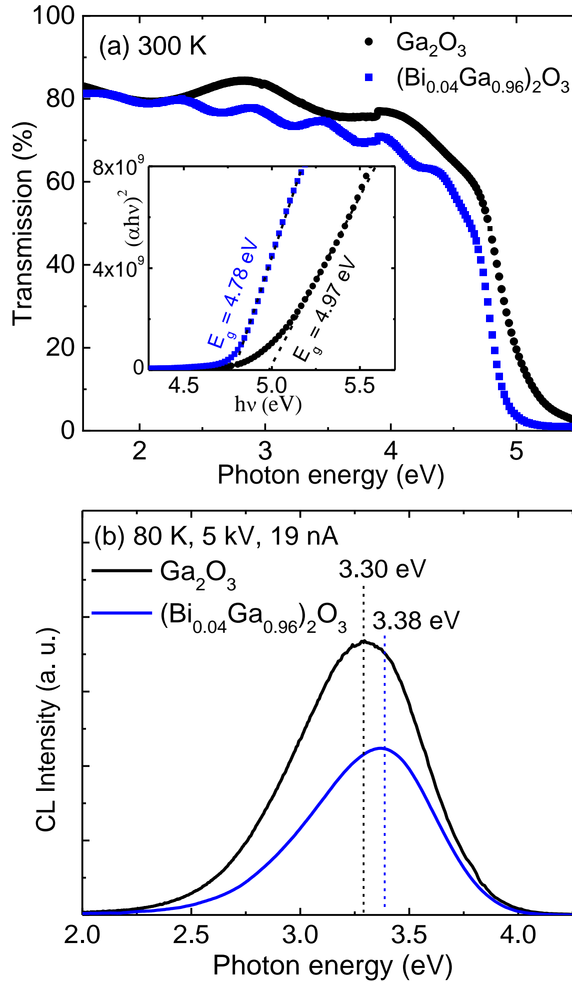

Figure 2. (a) Optical transmission spectra of the Ga_2O_3 and the $(Bi_{0.04}Ga_{0.96})_2O_3$ films at 300 K showing an optical transmittance of ~ 80% in the visible range. Inset: linear fitting of the Tauc plot yields a bandgap of 4.97 and 4.78 ± 0.03 eV for the Ga_2O_3 and $(Bi_{0.04}Ga_{0.96})_2O_3$ films, respectively. (b) CL spectra of the Ga_2O_3 and $(Bi_{0.04}Ga_{0.96})_2O_3$ films acquired at 80 K. Alloying of the Ga_2O_3 with Bi_2O_3 leads to a decrease in the overall luminescence intensity by one third and a blue peak shift of 80 meV.

The optical transmission spectrum of the Ga_2O_3 film, depicted in Figure 2(a), exhibits a transmission of ~ 80% in the visible range, comparable with the films grown on sapphire substrates by metal-organic chemical vapor deposition (MOCVD) [17]. The $(Bi_{0.04}Ga_{0.96})_2O_3$ film unveils slightly lower transmission compared with the nominally undoped film, likely due to Bi-induced

formation of defects within the bandgap. In the UV range, both the Ga_2O_3 and $(Bi_{0.04}Ga_{0.96})_2O_3$ films exhibit a sharp fundamental absorption edge. The Tauc plot, displayed in the inset, yields a bandgap energy of 4.97 ± 0.10 eV for Ga_2O_3 and a smaller bandgap of 4.78 ± 0.10 eV for $(Bi_{0.04}Ga_{0.96})_2O_3$. The bandgap narrowing can be attributed to the formation of an intermediate VB composed of Bi 6s and O 2p orbitals, consistent with the results from DFT calculations of dilute $(Ga_{1-x}Bi_x)_2O_3$ by Cai *et al.* [14]. For the x fraction equal to 0.04 in this work, this intermediate band is situated at 0.2 eV above the Ga_2O_3 VB. The CL spectra of the Ga_2O_3 and $(Bi_{0.04}Ga_{0.96})_2O_3$ films are presented in Figure 2(b). The emission intensity of the $(Bi_{0.04}Ga_{0.96})_2O_3$ is about 30% lower than the Ga_2O_3 as the alloying can induce defects that participate in competitive non-radiative recombination channels. The Ga_2O_3 and $(Bi_{0.04}Ga_{0.96})_2O_3$ CL spectra at 80 K are peaked at 3.30 and 3.38 eV, respectively, showing a significant blue peak shift due to the Bi incorporation. This blue shift arises from weaker defect-related emissions in the $(Bi_{0.04}Ga_{0.96})_2O_3$ film compared with the nominally undoped Ga_2O_3 (see supplementary Figure S1 and discussed further below).

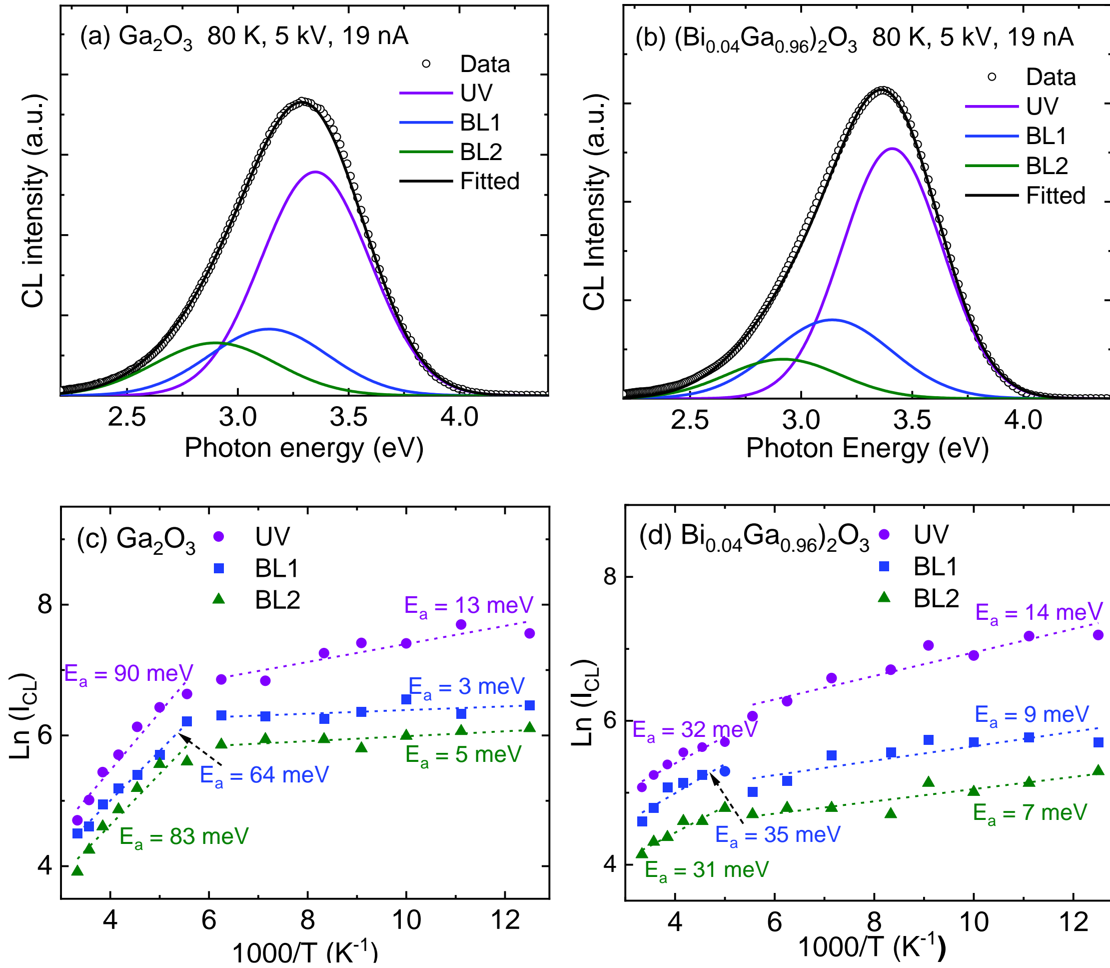

Figure 3. Gaussian deconvolution of CL spectra of (a) Ga_2O_3 and (b) $(Bi_{0.04}Ga_{0.96})_2O_3$ at 80 K using three Gaussian functions. Three emission bands UV (3.38-3.41 eV), BL1 (3.14 eV), and BL2 band (2.92 eV) are characteristic luminescence peaks in Ga_2O_3 luminescence [18, 19]. (c, d) Arrhenius plots of the ln (I_{CL}) as a function of 1000/T (K^{-1}) for the films with the activation energies obtained from the linear fits indicated within the graphs.

Both the self-trapped hole (STH) and defect-related peaks in Ga_2O_3 and its alloys of the monoclinic phase are expectedly broad due to strong electron-photon coupling producing highly overlapped emissions; accordingly spectral deconvolution is needed to extract meaningful results from their luminescence data [20]. The Gaussian peak fitting method is employed for spectral deconvolution as previously described for β-Ga_2O_3 [21]. Using this approach, the CL spectra of the Ga_2O_3 film are fitted with three luminescence bands centered at 3.38 eV (UV), 3.14 eV (BL1) and

2.92 eV (BL2) with a respective full width at half maximum (FWHM) of ~0.60, 0.65 and 0.66 eV. The UV peak is characteristic of β-Ga_2O_3 and originates from the radiative recombination of a free electron and a STH [18], while the two BL peaks are assigned to native defects involving a donor V_O or Ga interstitial (Ga_i) and an acceptor either a V_{Ga} or a (V_O-V_{Ga}) complex [19, 22, 23]. Since the formation of (V_O-V_{Ga}) complex is more energetically favourable than V_{Ga}, it is more likely (V_O-V_{Ga}) acceptor is involved in the blue luminescence [24]. The CL spectra of $(Bi_{0.04}Ga_{0.96})_2O_3$ could also be adequately fitted with three Gaussian peaks, which are centered at the 3.41 eV (UV), 3.14 eV (BL1) and 2.92 eV (BL2) with FWHM of 0.59, 0.6 and 0.65 eV, respectively. It is worth noting that there is a significant blue shift in the overall spectrum of $(Bi_{0.04}Ga_{0.96})_2O_3$ compared with that of Ga_2O_3 at a given temperature [see Figure 2(b)]. This blue shift is caused by the quenching of the defect-related bands relative to the intrinsic STH due to the Ga_2O_3 alloying. Supplementary Figure S1 shows the relative peak areas of BL1 and BL2 bands for the two films from 80 to 300 K, which reveals their intensities in $(Bi_{0.04}Ga_{0.96})_2O_3$ are approximately 20 – 50% lower than in Ga_2O_3 at a given temperature below 200 K. The reduction of the V_{Ga} density in the film upon Bi_2O_3 alloying can be explained by the suppression of defect formation because the growth conditions become more cation-rich with the addition of Bi vapor during the growth.

Table 1. Activation energies of the UV, BL1 and BL2 CL emission bands of the Ga_2O_3 and $(Bi_{0.04}Ga_{0.96})_2O_3$ films deduced from the Arrhenius analysis of their integrated intensities.

	Activation energy (meV)			
	Ga_2O_3		$(Bi_{0.04}Ga_{0.96})_2O_3$	
Peak	80-160 K	180-300 K	80-180 K	200-300K
UV (3.36-3.41) eV	13 ± 2	90 ± 4	14 ± 2	32 ± 5
BL1 3.14 eV	3 ± 1	64 ± 3	9 ± 2	35 ± 7
BL2 2.92 eV	5 ± 1	83 ± 3	7 ± 2	31 ± 4

All the UV, BL1 and BL2 bands in both films are quenched with increasing temperature and Arrhenius analysis using their integrated intensities obtained from the curve fitting is performed to determine the activation energy of their electronic transitions as presented in Figure 3(c, d). Linear regression of the Arrhenius plots ln(I_{CL}) versus 1000/T (K^{-1}) for the Ga_2O_3 and $(Bi_{0.04}Ga_{0.96})_2O_3$ films reveal two regions with different activation energies (E_a). The resultant activation energies are summarised in Table 1. In Ga_2O_3, at temperatures below 160 K, the BL peaks centered at 3.14 eV and 2.92 eV have E_a values of 3 ± 1 and 5 ± 1 meV, respectively; these weak temperature dependences of the emissions are likely associated with phonon-assisted excitation of the localized defects. At temperatures above 160 K, the E_a of the BL1 and BL2 peaks increase to 64 ± 3 and 83 ± 3 meV, respectively. While the E_a of the UV peak increases from 13 ± 2 meV under 160 K to 90 ± 4 meV above 160 K. The E_a values of the UV, BL1 and BL2 bands of the $(Bi_{0.04}Ga_{0.96})_2O_3$ are obtained over two temperature regions of 80 to 180 K and 200 to 300 K. The E_a of the UV peak in the higher temperature region is 32 ± 5 meV while the E_a of the BL1 and BL2 are 35 ± 7 meV and 31 ± 4 meV, respectively. The chemical nature of defects and impurities responsible for these BL bands in Ga_2O_3 has not been conclusively identified in the literature; our temperature dependent results show that their ionization energies are lowered in $(Bi_{0.04}Ga_{0.96})_2O_3$ due to the up-shift of the valence band. Remarkably, the E_a of the UV band after alloying decreases from 90 ± 4 eV in Ga_2O_3 to 32 ± 5 meV in $(Bi_{0.04}Ga_{0.96})_2O_3$. This result indicates that alloying Ga_2O_3 with Bi_2O_3 lowers the hole self-trapping energy, decreasing the thermal stability of STHs in $(Bi_{0.04}Ga_{0.96})_2O_3$. The temperature-resolved spectra of the Ga_2O_3 and $(Bi_{0.04}Ga_{0.96})_2O_3$ films for temperatures above 200 K are presented in supplementary Figure S2, showing that the STH emission intensity in Ga_2O_3 decreases by a factor of 4 with rising temperature from 200 to 300 K. The STH intensity in $(Bi_{0.04}Ga_{0.96})_2O_3$, on the other hand, decreases by a factor of about 7 over the same temperature range due to lower thermal stability of STHs.

3.3 Influence of Bi_2O_3 alloying on the electrical and dielectric properties

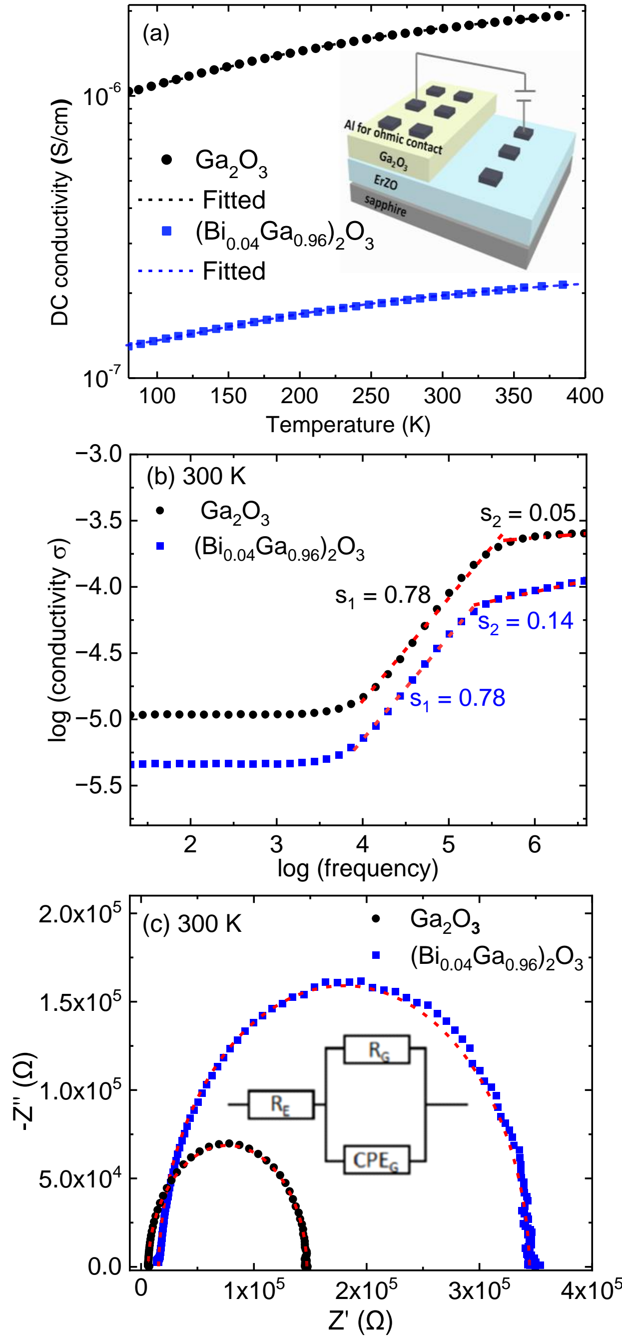

Figure 4. (a) Temperature-dependent DC conductivity of the Ga_2O_3 and $(Bi_{0.04}Ga_{0.96})_2O_3$ films over a range of 80 – 400 K, showing the conductivity is reduced by an order of magnitude after alloying Ga_2O_3 with Bi_2O_3. Inset shows the device structure used for the electrical measurements in this work. (b) Double logarithmic plot of the AC conductivity versus frequency for the films at 300 K. The frequency-dependent conductivity is fitted using the Jonscher power law, yields the indicated exponent S values over the lower (< 10^6 Hz) and upper (> 10^6 Hz) frequency ranges. (c) Nyquist plots for the films together the equivalent circuit used for their simulation.

Temperature-dependent DC conductivity of the Ga_2O_3 and $(Bi_{0.04}Ga_{0.96})_2O_3$ films is presented in Figure 4(a). The device structure used for the measurements of electrical and dielectric properties is also depicted in this figure; the Ohmic contact is realized by using an array of Al electrodes on the film surface. As the temperature is elevated from 80 to 400 K, the DC conductivity is found to increase from 1.0×10^{-6} to 1.9×10^{-6} S/cm, and from 1.3×10^{-7} to 2.1×10^{-7} S/cm for the Ga_2O_3 and $(Bi_{0.04}Ga_{0.96})_2O_3$ films, respectively. The DC conductivity data are fitted according to the Arrhenius relation $\sigma_{DC} = \sigma_o \exp\left(-\frac{E_{ai}}{kT}\right)$, where E_{ai} is the electrical activation energy and σ_o is a constant. The data from the Ga_2O_3 and $(Bi_{0.04}Ga_{0.96})_2O_3$ films are well fitted to this equation with $E_{ai} = 26 \pm 2$ meV, indicating that the conduction is predominantly governed by the thermal activation of a shallow donor state, with Si or Ge impurities being the most likely candidates [2, 21]. There is a substantial decrease in the film conduction following Bi_2O_3 alloying, with the DC conductivity of $(Bi_{0.04}Ga_{0.96})_2O_3$ being one order of magnitude lower than that of Ga_2O_3 over the entire temperature range. The lower conductivity of the $(Bi_{0.04}Ga_{0.96})_2O_3$ film can be attributed to a reduction in the free carrier concentration as shallow donors are compensated by the activation of acceptors due to the formation of the Bi_2O_3-induced higher energy VB [14]. Hall effect measurements were attempted using a NanoMagnetics Instruments ezHEMS system with a measurement limit of 10^9 Ω.cm; however, the carrier concentration in the films could not be measured reliably due to their high resistivity. The AC conductivity of the films over the wide frequency range from 20 Hz to 10 MHz is shown in Figure 4(b). The frequency dependence of the film conductivity is weak in the low frequency region below 3 kHz and the plateau region shows the film conductivity is lowered by an order of magnitude in the $(Bi_{0.04}Ga_{0.96})_2O_3$ film, consistent with the DC results. The AC conductivity rises with increasing frequency as expected and the data can be fitted according to the Jonscher's power law, $\sigma(f) = \sigma_{DC} + \sigma_o . f^s$, where σ_{DC} is the DC conductivity, σ_o is the pre-factor related to the strength of polarizability and s is the frequency exponent reflecting the nature of electrical relaxation [25, 26].

As shown in the double logarithmic plot of $\sigma(f)$ versus frequency, the AC behavior is characterized by two relaxation processes with different s values. In the frequency range of $10^4 - 10^6$ Hz, $s_1 = 0.78 \pm 0.02$ is obtained from the linear fitting, indicating that the correlated barrier hopping mechanism between donor states is responsible for the AC conduction in both films [15]. The identical s_1 exponent for the Ga_2O_3 and $(Bi_{0.04}Ga_{0.96})_2O_3$ films indicates the barrier energy for electron hopping is the same and the electron conduction mechanism is unaltered by the formation of the Bi-related intermediate VB band [27]. In the upper frequency range $f > 10^6$ Hz, s_2 is close to zero for Ga_2O_3. Conversely, the measured $s_2 = 0.14$ for $(Bi_{0.04}Ga_{0.96})_2O_3$ is significantly different from zero, which reflects a different interaction of carriers with the introduced Bi ions in the alloy [28].

Figure 4(c) shows the complex impedance spectra of the Ga_2O_3 and $(Bi_{0.04}Ga_{0.96})_2O_3$ films in the form of the Nyquist plot featuring counterclockwise semicircles. The larger diameter of the $(Bi_{0.04}Ga_{0.96})_2O_3$ Nyquist semicircle indicates an increased total resistance, consistent with the conductivity results shown in Figure 4(a, b). The impedance spectra are fitted using Scribner's ZView software with an equivalent circuit consisting of a resistive electrode resistance (R_E) and parallel R_G-CPE_G elements connected in series as shown in the inset of Figure 4(c), where R_G is the grain boundary resistance. CPE_G is the constant phase element, which is used instead of a pure capacitor because the material is not an ideal Debye system. The fitted values for the three components are: $R_E = 6.4 \times 10^3\ \Omega$, $R_G = 1.4 \times 10^5\ \Omega$ and $CPE_G = 0.12$ nF for Ga_2O_3, and $R_E = 1.5 \times 10^4\ \Omega$, $R_G = 3.3 \times 10^5\ \Omega$ and $CPE_G = 0.067$ nF for $(Bi_{0.04}Ga_{0.96})_2O_3$. CPE values in the order of nF is typically ascribed to the capacitance of grain boundaries. The increased R_G and lowered CPE_G for $(Bi_{0.04}Ga_{0.96})_2O_3$ compared with those of Ga_2O_3 suggest larger grain sizes due to the Bi_2O_3 alloying. A similar effect is observed in other oxides where the grain boundary resistance and capacitance respectively increase and decrease with increasing grain size up to ~ 300 nm [29, 30]. These results are consistent with the grain size enlargement induced by the Bi_2O_3 alloying as reported above from AFM and XRD

measurements. The performance of the films as dielectric materials is shown in supplementary Figure S3 where the dielectric constant (ε) and dielectric loss ($tan\delta$) are displayed as a function of driving voltage frequency. Similar frequency dependencies are observed for the Ga_2O_3 and $(Bi_{0.04}Ga_{0.96})_2O_3$ films over the entire measured frequency range of 20 Hz to 10 MHz, confirming that the Bi_2O_3 alloying does not significantly alter the crystal structure or ionic polarization mechanism in Ga_2O_3. At 1 kHz, $\varepsilon = 16.5$ and $tan\delta = 11.5$ for the Ga_2O_3 film and $\varepsilon = 11.5$ and $tan\delta = 8.6$ for $(Bi_{0.04}Ga_{0.96})_2O_3$; these values reflect changes in the ionicity of the bonding due to the incorporation of Bi cations.

4. Conclusion

Monoclinic phase ternary alloys of Ga_2O_3 and Bi_2O_3 have been successfully fabricated using magneton co-sputtering. Detailed optical and electrical characterization studies of β-$(Bi_{0.04}Ga_{0.96})_2O_3$ reveal a shrinkage in the optical bandgap noted from 4.97 to 4.78 eV due to the Bi_2O_3 alloying, consistent with the theoretical prediction of the formation of an intermediate higher energy VB induced by Bi_2O_3 alloying. The $(Bi_{0.04}Ga_{0.96})_2O_3$ film exhibits a blueshift in its luminescence spectra compared Ga_2O_3 films; however, its UV luminescence band associated with self-trapped holes is shown to quench rapidly with increasing temperature, indicating the alloying lowers the self-trapping energy for holes in the $(Bi_{0.04}Ga_{0.96})_2O_3$ films. Electrical measurements show the DC and AC conductivities of the $(Bi_{0.04}Ga_{0.96})_2O_3$ film are about one order of magnitude lower than those measured in Ga_2O_3 films, which is attributed to the compensation of shallow donors due to the lower binding energy of acceptors as a result of the alloying-induced upward valence band shift. Impedance spectroscopy analysis reveals a decrease in both the film conductivity and capacitance for $(Bi_{0.04}Ga_{0.96})_2O_3$, which is consistent with the observed increase in the average grain size due to the Bi_2O_3 alloying.

CRediT authorship contribution statement

Fatima Matar: Investigation, Data curation, Formal analysis, Writing − original draft. **Ying-Li Shi:** Investigation, Data curation, Formal analysis. **Francis Chi-Chung Ling:** Conceptualization, Resources. **Amar Salih:** Investigation, Visualization. **Curtis P. Irvine**: Investigation, Validation. **Sujeewa De Silva:** Methodology, Supervision. **Matthew R. Phillips:** Methodology, Resources, Writing − review & editing. **Cuong Ton-That:** Conceptualization, Formal analysis, Project administration, Writing − review & editing.

Declaration of competing interest

The authors declare that they have no known competing financial interests or personal relationships that could have appeared to influence the work reported in this paper.

Data Availability

Data will be made available on request.

Acknowledgements

This work was supported under Australian Research Council (ARC) Discovery Project funding scheme (project DP210101146). The authors would like to thank Danica Solina, Herbert Yuan, Alexander Angeloski and James Bishop for technical support.

References

[1] S.J. Pearton, J. Yang, P.H. Cary, F. Ren, J. Kim, M.J. Tadjer, M.A. Mastro, A review of Ga2O3 materials, processing, and devices, Applied Physics Reviews, 5 (2018) 011301.

[2] K. Irmscher, Z. Galazka, M. Pietsch, R. Uecker, R. Fornari, Electrical properties of β-Ga2O3 single crystals grown by the Czochralski method, Journal of Applied Physics, 110 (2011) 063720.

[3] T.T. Huynh, E. Chikoidze, C.P. Irvine, M. Zakria, Y. Dumont, F.H. Teherani, E.V. Sandana, P. Bove, D.J. Rogers, M.R. Phillips, C. Ton-That, Red luminescence in H-doped β−Ga2O3, Physical Review Materials, 4 (2020) 085201.

[4] V. Patil, B.-T. Lee, S.-H. Jeong, Optical and structural characterization of high crystalline β-Ga_2O_3 films prepared using an RF magnetron sputtering, Journal of Alloys and Compounds, 894 (2022) 162551.

[5] A.T. Neal, S. Mou, S. Rafique, H. Zhao, E. Ahmadi, J.S. Speck, K.T. Stevens, J.D. Blevins, D.B. Thomson, N. Moser, Donors and deep acceptors in β-Ga_2O_3, Applied Physics Letters, 113 (2018) 062101.

[6] A. Mauze, Y. Zhang, T. Itoh, E. Ahmadi, J.S. Speck, Sn doping of (010) β-Ga_2O_3 films grown by plasma-assisted molecular beam epitaxy, Applied Physics Letters, 117 (2020) 222102.

[7] C. Yan, J. Su, Y. Wang, Z. Lin, J. Zhang, J. Chang, Y. Hao, Reducing the acceptor levels of p-type β-Ga_2O_3 by (metal, N) co-doping approach, Journal of Alloys and Compounds, 854 (2021) 157247.

[8] F. Zhang, K. Saito, T. Tanaka, M. Nishio, M. Arita, Q. Guo, Wide bandgap engineering of $(AlGa)_2O_3$ films, Applied Physics Letters, 105 (2014) 162107.

[9] H. Von Wenckstern, D. Splith, M. Purfürst, Z. Zhang, C. Kranert, S. Müller, M. Lorenz, M. Grundmann, Structural and optical properties of $(In, Ga)_2O_3$ thin films and characteristics of Schottky contacts thereon, Semiconductor Science and Technology, 30 (2015) 024005.

[10] S. Seacat, J.L. Lyons, H. Peelaers, Properties of orthorhombic Ga_2O_3 alloyed with In_2O_3 and Al_2O_3, Applied Physics Letters, 119 (2021) 042104.

[11] D. Song, L. Li, B. Li, Y. Sui, A. Shen, Band gap engineering of N-alloyed Ga_2O_3 thin films, AIP Advances, 6 (2016) 065016.

[12] C.S. Chang, N. Tanen, V. Protasenko, T.J. Asel, S. Mou, H.G. Xing, D. Jena, D.A. Muller, γ-phase inclusions as common structural defects in alloyed β-$(Al_xGa_{1-x})_2O_3$ and doped β-Ga_2O_3 films, APL Materials, 9 (2021) 051119.

[13] T. Oshima, S. Fujita, Properties of Ga_2O_3-based $(In_x Ga_{1-x})_2O_3$ alloy thin films grown by molecular beam epitaxy, Physica Status Solidi C, 5 (2008) 3113-3115.

[14] X. Cai, F.P. Sabino, A. Janotti, S.-H. Wei, Approach to achieving a p-type transparent conducting oxide: Doping of bismuth-alloyed Ga_2O_3 with a strongly correlated band edge state, Physical Review B, 103 (2021) 115205.

[15] Y.-L. Shi, D. Huang, F.C.-C. Ling, Q.-S. Tian, L.-S. Liao, M.R. Phillips, C. Ton-That, Correlation between small polaron tunneling relaxation and donor ionization in Ga_2O_3, Applied Physics Letters, 120 (2022) 172105.

[16] S. Nakagomi, Y. Kokubun, Crystal orientation of β-Ga_2O_3 thin films formed on c-plane and a-plane sapphire substrate, Journal of Crystal Growth, 349 (2012) 12-18.

[17] D. Hu, S. Zhuang, Z. Ma, X. Dong, G. Du, B. Zhang, Y. Zhang, J. Yin, Study on the optical properties of β-Ga_2O_3 films grown by MOCVD, Journal of Materials Science: Materials in Electronics, 28 (2017) 10997-11001.

[18] Y.S. Wang, P.T. Dickens, J.B. Varley, X.J. Ni, E. Lotubai, S. Sprawls, F. Liu, V. Lordi, S. Krishnamoorthy, S. Blair, K.G. Lynn, M. Scarpulla, B. Sensale-Rodriguez, Incident wavelength and polarization dependence of spectral shifts in beta-Ga2O3 UV photoluminescence, Sci. Rep., 8 (2018) 18075.

[19] T. Onuma, S. Fujioka, T. Yamaguchi, M. Higashiwaki, K. Sasaki, T. Masui, T. Honda, Correlation between blue luminescence intensity and resistivity in β-Ga2O3 single crystals, Applied Physics Letters, 103 (2013) 041910.

[20] T. Huynh, L. Lem, A. Kuramata, M. Phillips, C. Ton-That, Kinetics of charge carrier recombination in β−Ga2O3 crystals, Physical Review Materials, 2 (2018) 105203.

[21] C.P. Irvine, A. Stopic, M.T. Westerhausen, M.R. Phillips, C. Ton-That, Enhancement of excitonic and defect-related luminescence in neutron transmutation doped β−Ga2O3, Physical Review Materials, 6 (2022) 114603.

[22] K. Yamamura, L. Zhu, C.P. Irvine, J.A. Scott, M. Singh, A. Jallandhra, V. Bansal, M.R. Phillips, C. Ton-That, Defect Compensation in Nitrogen-Doped β-Ga2O3 Nanowires: Implications for Bipolar Nanoscale Devices, ACS Applied Nano Materials, 5 (2022) 12087-12094.

[23] M.D. McCluskey, Point defects in Ga2O3, Journal of Applied Physics, 127 (2020) 101101.

[24] Y.K. Frodason, K.M. Johansen, L. Vines, J.B. Varley, Self-trapped hole and impurity-related broad luminescence in β-Ga2O3, Journal of Applied Physics, 127 (2020) 075701.

[25] A.K. Jonscher, The 'universal'dielectric response, Nature, 267 (1977) 673-679.

[26] S. Elliott, AC conduction in amorphous chalcogenide and pnictide semiconductors, Advances in Physics, 36 (1987) 135-217.

[27] Y.-L. Shi, D. Huang, U. Kentsch, S.-Q. Zhou, F.C.-C. Ling, A high-k Cu-doped ZnO film formed via Ga-ion implantation: The acceptor-donor co-doping approach, Journal of Alloys and Compounds, 911 (2022) 165057.

[28] A. Dhahri, E. Dhahri, E. Hlil, Electrical conductivity and dielectric behaviour of nanocrystalline La0.6Gd0.1Sr0.3 Mn0.75Si0.25O3, RSC Advances, 8 (2018) 9103-9111.

[29] V. Ivanov, S. Shkerin, A. Rempel, V. Khrustov, A. Lipilin, A. Nikonov, The grain size effect on the yttria stabilized zirconia grain boundary conductivity, Journal of Nanoscience and Nanotechnology, 10 (2010) 7411-7415.

[30] S. Yang, Y. Ping, L. Qian, J. Han, B. Xiong, J. Li, P. Fang, C. He, Flower-like Bi2O3 with enhanced rate capability and cycling stability for supercapacitors, Journal of Materials Science: Materials in Electronics, 31 (2020) 2221-2230.